THE JOURNAL OF PHYSICAL CHEMISTRY B

Article

pubs.acs.org/JPCB

Restricted Puckering of Mineralized RNA-Like Riboses

J. Casanovas,[†] G. Revilla-López,[‡] O. Bertran,[§] L. J. del Valle,[‡] P. Turon,[∥,*] J. Puiggalí,[‡,⊥] and C. Alemán[‡,⊥,*]

[†]Departament de Química, Escola Politècnica Superior, Universitat de Lleida, c/Jaume II no. 69, Lleida E-25001, Spain

[‡]Departament d'Enginyeria Química, E. T. S. d'Enginyeria Industrial de Barcelona, Universitat Politècnica de Catalunya, Diagonal 647, 08028 Barcelona, Spain

[§]Departament de Física Aplicada, EEI, Universitat Politècnica de Catalunya, Pça. Rei 15, 08700 Igualada, Spain

[∥]B. Braun Surgical, S.A. Carretera de Terrasa 121, 08191 Rubi (Barcelona), Spain

[⊥]Center for Research in Nano-Engineering, Universitat Politècnica de Catalunya, Campus Sud, Edifici C', C/Pasqual i Vila s/n, Barcelona E-08028, Spain

ABSTRACT: The pseudorotational motions of highly hydroxylated pentafuranose sugars in the free state and tethered to hydroxyapatite have been compared. The conformation pentafuranose ring remains restricted at the North region of the pseudorotational wheel, which is the one typically observed for nucleosides and nucleotides in the double helix A-RNA, when the phosphate-bearing sugar is anchored to the mineral surface. Results indicate that the severe restrictions imposed by the mineral are responsible of the double helix preservation when DNA and RNA are encapsulated in crystalline nanorods.

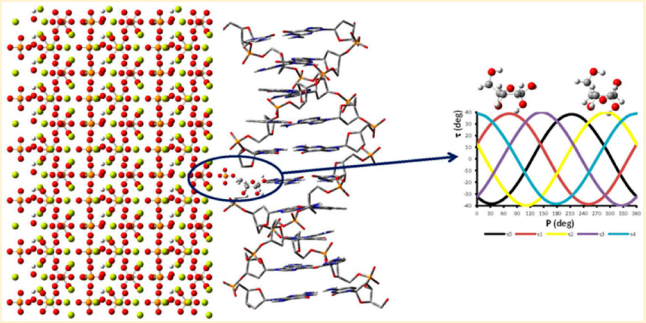

INTRODUCTION

Hydroxyapatite (HAp) has been a widespread building material in nature for millions of years.[1,2] Furthermore, since several decades ago, a number of biotechnological applications for nucleic acids (NA) separation and chemical protection have been reported. These are based in NA-HAp interactions at two complementary levels: HAp surface facets and NA-templated HAp nucleation.[1,2] The HAp-induced structural stabilization of the NAs has been suggested as a consequence of mineralization and the mechanism by which NAs are protected from chemical degradation. Only recently, the role of NA phosphate as a HAp crystallization promoter, an part of the mineral, has been revealed at atomic-level.[3,4] Further, NA flexibility is tightly bound to ribose and 2′-deoxyribose sugars conformational variability as reported for different chemical modifications[5,6] but little is known about its behavior when phosphate is embedded in the HAp crystal (i.e., the latter creates a rigid inflexible wall containing the phosphates of the biomolecules and the mineral). This rigidity can be transferred to the rest of the NAs through changes in the flexibility of their sugars, an aspect which is totally unknown.

Traditionally, the flexibility of pentofuranose sugars is described using the concept of pseudorotation (Figure 1), which allows unequivocal determination of the exact conformation of each five-membered ring in terms of two parameters, the phase of pseudorotation (P) and the puckering amplitude (τ_m).[7,8] Both P and τ_m are defined by endocyclic torsion angles (Figure 2). As canonical and noncanonical segments of functional DNA and RNA duplexes are influenced by sugar pucker conformations,[9−11] work in this field has been essentially focused on the comparison of the pseudorotational equilibrium between abasic sugars and nucleosides.[7,8,12−21] In addition, sugars puckering is expected influence the hydrolysis of N-glycosidic bond.[22]

In this work, we investigate the relationship between the sugar conformation and HAp. In particular, we are interested in highly hydroxylated pentafuranoses, which remain relatively unknown. As a first step, molecular modeling tools have been used as in our previous B-DNA study[3] to check that A-type RNA double helices can be encapsulated inside nanopores of crystalline HAp, $Ca_{10}(PO_4)_6(OH)_2$ and hexagonal symmetry,[23] without undergoing significant alterations in the secondary structure. After this, the influence of the inorganic environment on the pseudorotational movement has been investigated. For this purpose, the pseudorotational spaces of β-D-ribofuranose (denoted **1** in Scheme 1), a pentafuranose ring bearing four hydroxyl groups, β-D-ribofuranose 5-phosphate (denoted **2** in Scheme 1), in which the hydroxyl group attached to the exocyclic methylene unit is replaced by a phosphate group, and **2** anchored to a HAp mineral wall have been determined using density functional theory (DFT) calculations.

METHODS

Force-Field Simulations. Both energy minimization and MD simulations were applied using the NAMD 2.6 program.[24]

Received: February 18, 2014
Revised: April 20, 2014
Published: May 1, 2014

dx.doi.org/10.1021/jp501714q | J. Phys. Chem. B 2014, 118, 5075−5081

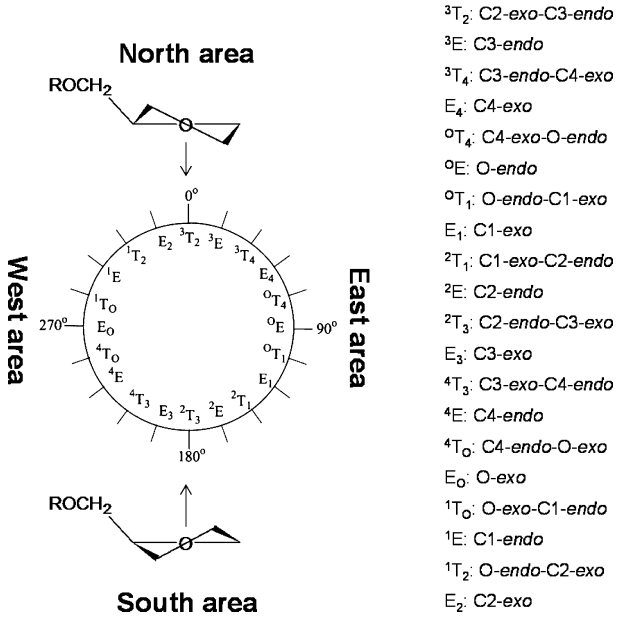

Figure 1. Pseudorotational wheel of pentafuranose sugars (left). The *North*, *East*, *South*, and *West* regions are defined. Description of the conformations associated with the twist and envelope arrangements of the pentafuranose ring is also provided (right).

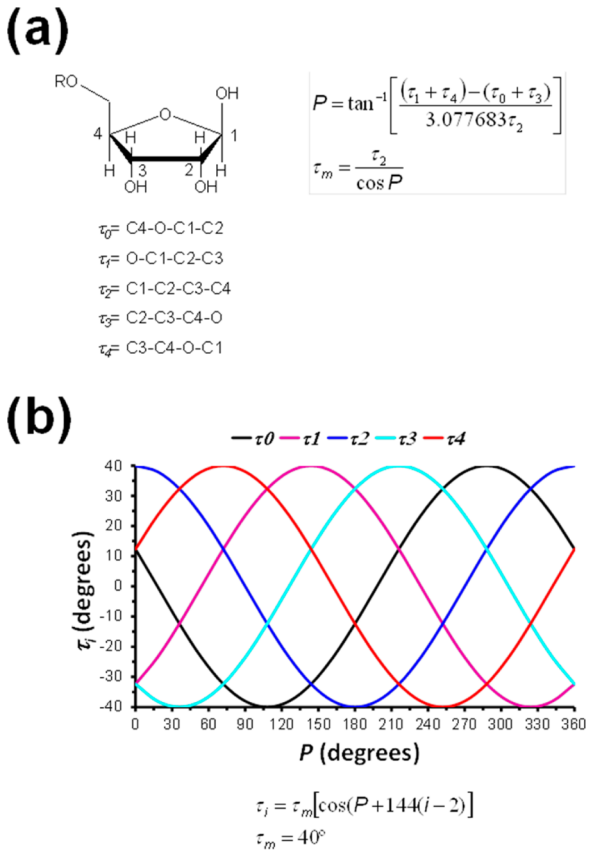

Figure 2. (a) Endocyclic dihedral angles of pentafuranose sugars and expressions used to obtain the phase of pseudorotation (P) and the puckering amplitude (τ_m). (b) Variation of the endocyclic torsional angles with P (τ_m was set to 39°).

Models constructed to examine the stability of the A-RNA double helix embedded into HAp nanopores were minimized by applying 5×10^3 steps of steepest descent to relax the more important conformational and structural tensions. Then, a MD run of 3.0 ns in the *NVT* ensemble (constant number of particles, volume and temperature) at 298 K was carried out to equilibrate the systems and eliminate small structural tensions. After such thermal relaxation, the saved coordinates were submitted to a new energy minimization by applying 5×10^3 steps of steepest descent. In both energy minimizations and MD simulation, atoms contained in A-RNA were only allowed to move from their positions, the coordinates of the mineral being kept fixed at their crystallographic positions in all cases. It should be emphasized that all the systems were calculated in triplicate considering starting points that differ in the orientation of the A-RNA with respect to the apatite.

Scheme 1

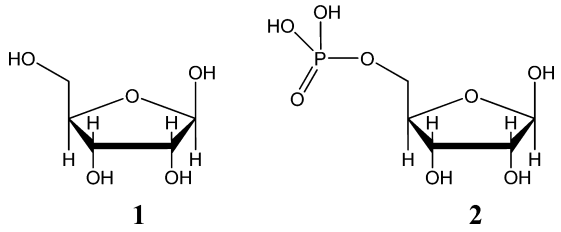

The potential energy was computed using the Amber force-field.[25] All force-field parameters for DNA as well as the phosphate and hydroxyl groups were extracted from Amber ff03.[26] It should be noted that the ff03 parameters are identical to the ff99-SB[27] ones for nucleic acids, phosphate and hydroxyl groups. Force-field parameters of Ca^{2+} were extracted from the work reported by Bradbrook et al.[28] The ability of this set of force-field parameters to reproduce the inorganic···organic interactions found in biominerals was recently proved.[3]

Puckering pseudorotation angles, P, and amplitudes, τ_m, were determined following Altona and Sundaralinga,[7,8] (Figure 2a), using the same reference state for $P = 0.0°$. The pseudorotation space is divided into four equally sized quadrants, centered around $P = 0.0°$, $P = 90.0°$, $P = 180.0°$, and $P = 270.0°$, which are referred to as the *North*, *East*, *South*, and *West* quadrants (Figure 1), respectively. Structures to explore the pseudorotational properties were between $P = 0°$ and $P = 360°$ at 18° increments. Initially, dihedral angles internal to the ring were obtained using the formula displayed in Figure 2b,τ_m being set to 39°. In addition to the pseudorotational angle P, model sugars **1** and **2** contain several torsion angles associated with exocyclic groups for which different conformations are possible. For each of the 20 ring dispositions generated to examine the pseudorotation movements, different structures were constructed by varying such dihedral angles associated with the exocyclic moieties to form stabilizing O−H···O hydrogen bonds. A total of 8, 14, and 6 structures were generated for each ring disposition of **1**, **2**, and **2** tethered to HAp, respectively. Accordingly, the number of starting structures for geometry optimization were $20 \times 8 = 160$, $20 \times 14 = 280$ and $20 \times 6 = 120$, respectively.

The endocyclic dihedrals τ_0 and τ_1 were constrained during geometry optimization to ensure the pentafuranose conformation, all other parameters being freely optimized. All quantum mechanical calculations were carried out with the Gaussian 09 program[29] using the 6-311++G(d,p)[30,31] and 6-31G(d)[32] basis sets All pseudorotational energy surfaces were investigated at the DFT level of theory using a functional that combines the Becke's three-parameter hybrid functional (B3)[33] with the Lee, Yang, and

dx.doi.org/10.1021/jp501714q | J. Phys. Chem. B 2014, 118, 5075−5081

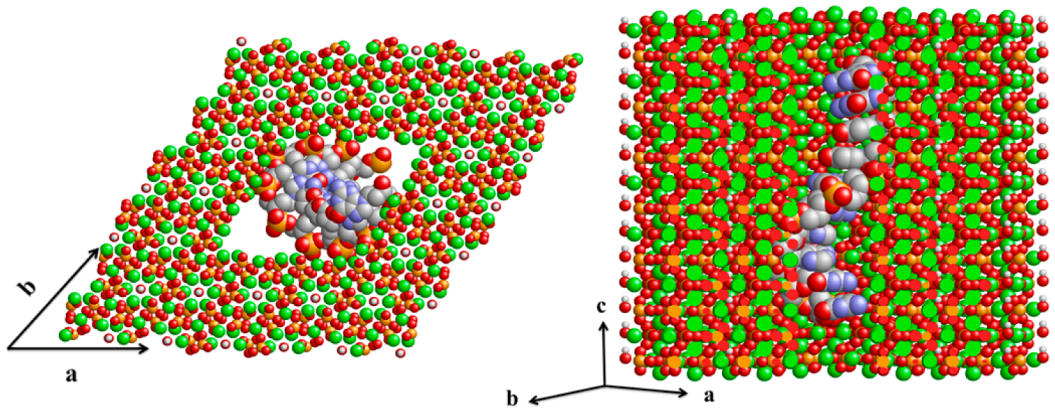

Figure 3. Equatorial and axial projections of the biomineral obtained by embedding helical A-RNA into a HAp nanopore. Calcium is represented in green, phosphorus in orange, oxygen in red, nitrogen in blue, and hydrogen of HAp hydroxyl groups in white (hydrogen atoms belonging to the RNA have been omitted).

Parr (LYP)[34] expression for the nonlocal correlation (B3LYP). The influence of dispersion forces in the pseudorotational profile of **2** tethered to HAp was evaluated by including single point Grimme's empirical dispersion correction for dispersion[35−37] at the B3LYP/6-31G(d) optimized geometries. To avoid an overestimation of dispersion effects, the C6 coefficient for Ca^{2+} was set to zero.[38]

RESULTS AND DISCUSSION

Natural hydroxyapatite (HAp) has a hexagonal crystal structure with space group $P6_3/m$ and periods $a = b = 9.42$ Å, and $c = 6.87$ Å.[23] The total number of atoms in the unit cell is 44, even though it only contains seven symmetrically independent atoms: two calcium ions, one forming single atomic columns parallel to the c axis and the other surrounding the hexagonal channel of hydroxyl in groups of the three calcium atoms at different heights; one phosphor and three oxygen atoms (forming PO_4^{3-} tetrahedral units; and the OH^- ions disordered along c about the mirror plane at $z = 1/4$. The occupancy of the OH^- sites was 50%, as necessary in a $P6_3/m$.

The chemical structure of the RNA dodecamer examined in this work is 5′-CGCGAAUUCGCG-3′, which corresponds to the Dickerson's dodecamer[39] used in our previous study[3] with DNA after replace thymine by uracile. This is a well-known sequence with three primary characteristic tracts: CG, AA and UU. The double helix was initially arranged in a typical A structure with pitch= 30 Å, 11 bases per turn, an axial rise of 2.79 Å and a base-pair tilt of 16.7°. Giving the hexagonal symmetry of HAp and the molecular dimensions of the A-RNA dodecamer, HAp model (supercell) was constructed considering $6 \times 6 \times 7$ unit cells. After this, a hole was generated in the center of the supercell, the dimensions of such hole being defined by the A-type double helix of RNA (i.e., steric conflicts between the apatite atoms and the A-RNA were not allowed). A hole of $2 \times 2 \times 7$ units cells was the minimum required to accommodate the double helix without severe steric contacts. In order to completely avoid unfavorable steric interactions between the HAp and the biomolecule, some additional atoms and groups of atoms were translated at their border regions allowing us to maintain the electroneutrality of the supercells. The side length of this hole is 19 Å and its angle γ is 120°. The resulting model (i.e., supercell with a hole of appropriated dimensions at the center) consists of 9856 atoms. In order to maintain the electrical neutrality of the system, Ca^{2+} ions were put at the minor groove of the RNA double helix. The positions of these ions were optimized by energy minimization while the coordinates of the rest of the atoms of the system were kept fixed.

Relaxation of the constructed models using MD simulations evidenced that encapsulation of the A-RNA double helix in constructed pores of HAp does not induce significant structural distortions in the secondary structure of the biomolecule (Figure 3). The diameter of the minimum pore needed to encapsulate A-RNA, which is defined by the shortest internal diagonal, is 21 Å. Integration of A-form RNA into HAp crystals is favored because four phosphate groups at the double helix are located at distances (i.e., ∼7 and ∼13) very similar to those identified for a crystallographic plane of the HAp structure (i.e., 6.87 and 11.66 Å), which results in stabilizing interactions between the Ca^{2+} atoms of HAp and the phosphate groups of RNA backbone. This expected result is fully consistent with both MD predictions and experimental observations on DNA-HAp biominerals, especially those involving nanocrystals.[3,4] On the other hand, the ribose rings of encapsulated A-RNA remained between the typical C2-*exo*-C3-*endo* ($^3T_2$) and C3-*endo* (^3E) conformations (i.e., *North* region of the pseudorotational wheel).

Since RNA-HAp biominerals share the most relevant characteristics observed for DNA-HAp, the rest of the work has focused on evaluating the influence of the mineral on the potential energy for pseudorotation. For this purpose, in a first stage the pseudorotational space of **1** has been scanned by constructing 20 different twist and envelope conformations, which differ in the endocyclic torsional angles used to define P since τ_m was set to 39° (Figure 2). For each of such 20 conformations, exocyclic hydroxyl groups were considered in 8 different dispositions, which result in structures that differ not only in the number of intramolecular hydrogen bonds but also in the their associated interaction pattern. All degrees of freedom other than the two endocyclic torsional angles used to preserve the P and τ_m values were optimized for the $20 \times 8 = 160$ structures at both B3LYP/6-31G(d) and B3LYP/6-311+G(d,p) levels.

Pseudorotational profiles for **1** were constructed considering the energy of the most stable structure for each value of P (Figure 4). Although the profiles obtained using the two basis sets are in excellent qualitative agreement, the flexibility of the furanose ring is considerably underestimated by the 6-31G(d) one. B3LYP/6-311+G(d,p) calculations corroborate the flexibility typically observed for all pentafuranose rings.[12−21] In spite of this common tendency, **1** presents features that are distinctive from

dx.doi.org/10.1021/jp501714q | J. Phys. Chem. B 2014, 118, 5075−5081

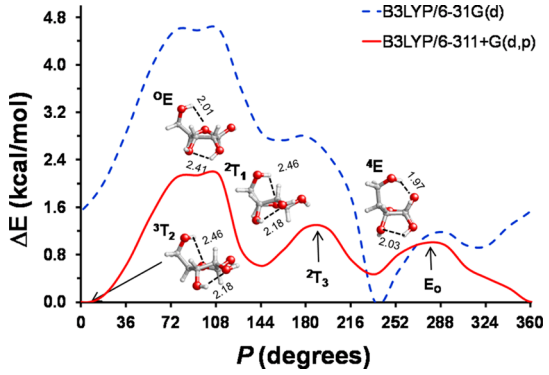

Figure 4. Pseudorotational energy curves calculated for **1**. Profiles were obtained through geometry optimization at the B3LYP/6-31G(d) and B3LYP/6-311+G(d,p) levels of 8 structures for each value of *P*, which ranged from 0° to 360° in steps of 18°. Energy profiles were constructed using the lowest energy structure for each value of *P*.

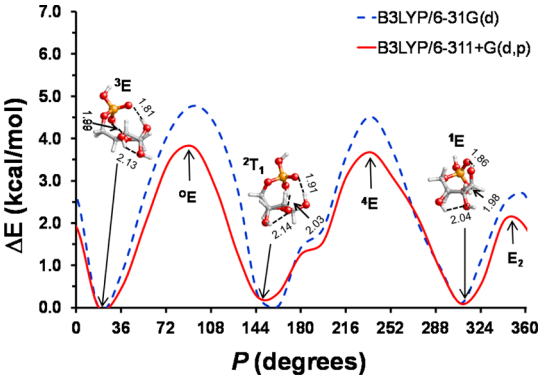

Figure 5. Pseudorotational energy curves calculated for **2**. Profiles obtained through geometry optimization at the B3LYP/6-31G(d) and B3LYP/6-311+G(d,p) levels of 14 structures for each value of *P*, which ranged from 0° to 360° in steps of 18°. These structures were constructed by varying the dihedral angles associated with the exocyclic moieties to form stabilizing O−H···O hydrogen bonds. Energy profiles were constructed using the lowest energy structure for each value of *P*.

less hydroxylated riboses and deoxyriboses. Three minima $^{3}T_{2}$ (P = 0.5°), $^{2}T_{1}$ (P = 144.7°) and ^{4}E (P = 235.4°) are clearly detected within a very narrow energy gap (<0.5 kcal/mol), the highest energy barrier (2.1 kcal/mol) corresponding to the ^{O}E (P = 93.4°). It should be noted that some X-ray and solution structures showing a ^{O}E sugar conformation were reported in early studies.[40,41] The positions of the three minima together with very low barriers found at the $^{2}T_{3}$ ($P \approx$ 180°) and E_{O} ($P \approx$ 270°) regions indicate that of pseudorotational motion associated with the *North* ($^{3}T_{2}$) ↔ *South* ($^{2}T_{1}$) interconversion occurs through *West* (^{4}E) conformations (the different areas are defined in Figure 1). In contrast, for less hydroxylayed surgars the *North* ↔ *South* interconversion proceeds through the East area.[12−21] This important difference has been essentially attributed to the stabilizing effect of hydrogen bonds involving the hydroxyl groups attached to the C2 and C3 of 1 as well as to the extra gauche effect associated with higher number of OCCO dihedrals.[12−21]

The same methodology was applied to evaluate the pseudorotational energy profile of **2**, the substitution of the C4′-hydroxyl by phosphate increasing considerably the number of hydrogen bonding groups with respect to **1**. Accordingly, the number of initial structures constructed by varying the orientation of the exocyclic groups for each arrangement of the pentafuranose ring increased from 8 to 14. Results obtained after optimization of such 20 × 14= 280 initial structures at the B3LYP/6-31G(d) and B3LYP/6-311+G(d,p) levels, which are displayed in Figure 5, reveal significant changes with respect to **1**. The $^{3}T_{2}$ and ^{4}E minima of **1** shift to ^{3}E (P = 18.1°) and ^{1}E (P = 308.7°), respectively, whereas the $^{2}T_{1}$ minimum remains (P = 145.1°). All these minima involve a hydrogen bonding network that is reinforced with respect to that found in **1** by strong phosphate···furarose interactions. Indeed each minimum presents two hydrogen bonds of such kind, the oxygen atoms of the phosphate moiety acting as donor in one and as acceptor in the other. Although the three minima are comprised within a relative energy gap of only 0.3 kcal/mol, they are separated by energy barriers of 3.8 (^{O}E, P = 94.5°), 3.7 (^{4}E, P = 235.7°) and 2.1 kcal/mol (E_{2}, P = 343.2°). These energy barriers are significantly higher than those detected for the interconversion between the minima of **1**, which has been attributed to the repulsive steric interactions provoked by the phosphate at some pseudorotational regions (i.e., the phosphate moiety is bulkier than the hydroxyl group of **1**). On the other hand, it is worth to mention the excellent agreement between the pseudorotational profiles calculated with the two basis sets, which in this case is not only qualitative but also quantitative. This result has allowed us to examine, as a next step, the influence of the biomineralization in the pseudorotational flexibility of **2** using the smallest basis set only.

The influence of HAp mineral in the flexibility of the sugar was evaluated by considering a complex model constructed by combining the information derived from both experiments on crystalline nanorods of HAp containing DNA molecules inside and MD simulations devoted to examine the templating effect of the biomacromolecule on the nucleation and growth of crystalline HAp.[4,40,41] Accordingly, the phosphate moiety of compound **2** was tethered to a mineral wall. Thus, the whole system, which involves 62 atoms, consists on a single HAp unit cell with the phosphate moiety of **2** embedded in the $(10\bar{1}0)$ facet (Figure 6a). This HAp wall restricts the number of initial structures with O−H···O hydrogen bonds that can be constructed for each arrangement of the pentafuranose ring, which decreases from 14 to 6, the resulting 6 × 20= 120 initial structures being optimized at the B3LYP/6-31G(d) level.

The pseudorotational profile displayed in Figure 6b shows two minima, $^{3}T_{2}$ (P = 0.6°) and $^{2}T_{3}$ (P = 179.8°), which were identified in the curve calculated for **1** (Figure 3) as a minimum and a barrier, respectively. However, both steric and electrostatic interactions induced by the ions of the HAp wall increase the energy gap between these two conformations from 1.3 to 5.4 kcal/mol. Thus, although the *North* ↔ *South* equilibrium identified for the sugar moiety of ribufuranosyl-*N*-nucleosides was the $^{3}T_{2}$ ↔ $^{2}T_{3}$,[7,8,12−21] the mineral practically vanishes the contribution of the $^{2}T_{3}$ conformation. Moreover, these two minima are separated by barriers at the *East* (^{O}E, P = 94.9°) and *West* ($^{4}T_{O}$, P = 255.0°) regions of 11.3 and 14.3 kcal/mol, respectively. It is worth noting that the $^{3}T_{2}$ minimum is fully consistent with the ribose conformations predicted by MD simulations for encapsulated A-RNA.

Dispersion forces may significant influence the pseudorotational profile of the calculated system. In order to evaluate this possibility, the previously discussed profile was refined by including single point Grimme's empirical correction for dispersion at the B3LYP/6-31G(d) optimized geometries. The

dx.doi.org/10.1021/jp501714q | J. Phys. Chem. B 2014, 118, 5075−5081

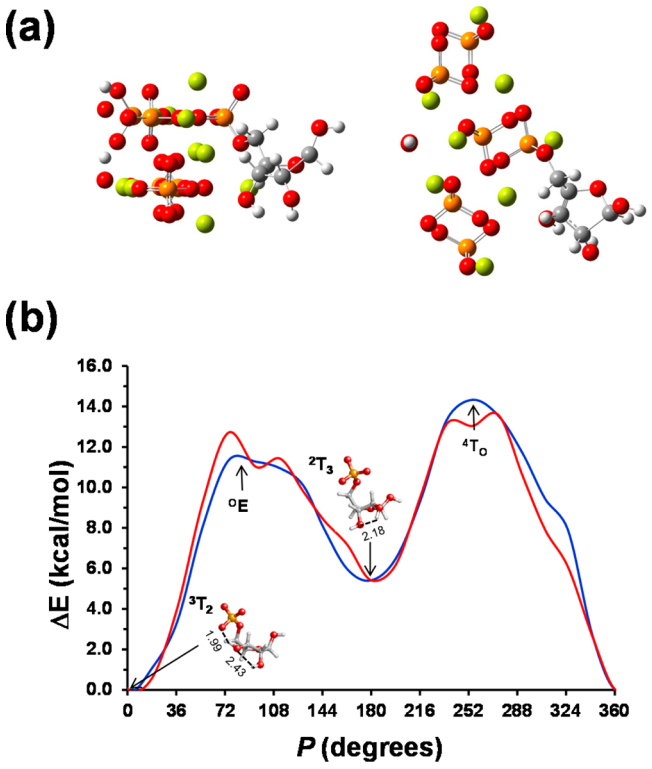

Figure 6. (a) Side (left) and upper (right) views of the model complex used to represent the tethering of **2** to a HAp wall (top). (b) Pseudorotational energy curves calculated for **2** tethered to a HAp wall. Initially, the profile was obtained through geometry optimization at the B3LYP/6-31G(d) level of six structures for each value of *P*, which ranged from 0° to 360° in steps of 18°. These structures were constructed by varying the dihedral angles associated with the exocyclic moieties to form stabilizing intramolecular hydrogen bonds. The B3LYP/6-31G(d) energy profile (blue curve) was constructed using the lowest energy structure for each value of *P*. The energy profile including dispersion curves (red curve) was obtained by including Grimme's correction for dispersion at the B3LYP geometries.

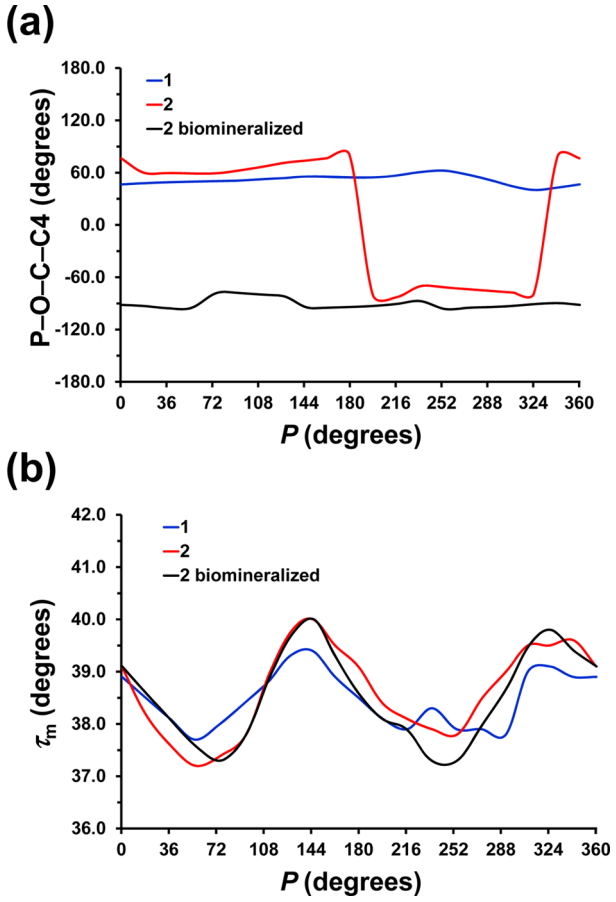

Figure 7. Variation of the (a) exocyclic dihedral angle P−O−C−C4 and (b) τ_m with *P* for **1** (B3LYP/6-311+G(d,p) geometries), **2** (B3LYP/6-311+G(d,p) geometries) and **2** tethered to a HAp wall (B3LYP/6-31G(d) geometries). In all cases the profiles were derived from the geometries used to represent the pseudorotational energy displayed in Figures 4, 5, and 6b.

resulting profile, which is included in Figure 6b, shows that dispersion forces do not affect the pseudorotational flexibility of the ring tethered to HAp. Accordingly, the overall results allow us to conclude that the pseudorotational flexibility of the sugar is practically inexistent when the double helix is embedded into the biomineral. Thus, the conformation pentafuranose ring remains restricted at the North region of the pseudorotational wheel, which is the one typically observed for nucleosides and nucleotides in the double helix A-RNA.

Figure 7a represents the variation of the exocyclic dihedral angle P−O−C−C4 with *P* obtained for **1**, **2** and **2** tethered to a HAp wall. Comparison of the profiles obtained for **2** in free-state and tethered to a HAp wall provides another prove of the drastic reduction provoked by biomineralization in the conformational flexibility of the sugar. Thus, the exocyclic dihedral angle of **2** shows *gauche*$^+$ → *gauche*$^-$ and *gauche*$^-$ → *gauche*$^+$ conformational transitions at $P \approx 180°$ and $P \approx 325°$, respectively. In contrast, the HAp wall precludes such conformational transitions, the exocyclic dihedral angle keeping a *gauche*$^-$ conformation during the whole pseudorotational profile. It should be noted that small conformational movements, as the amplitude of the five-membered ring, are not restricted by the HAp wall. This is evidenced in Figure 7b, which represents the variation of τ_m against *P* for the three calculated systems.

CONCLUSIONS

The flexibility of sugar rings of RNA and DNA used as templates for HAp crystallization is completely eliminated by the mineral. This contributes to preserve the secondary structure of the biomolecule and of the associated functionality. Highly hydroxylated riboses are extra-stabilized by intramolecular hydrogen bonds, which is fully consistent with very recent experimental observations on RNA double helices modified by extra-hydroxylation.

AUTHOR INFORMATION

Corresponding Authors

*(P.T.) E-mail: pau.turon@bbraun.com.
*(C.A.) E-mail: carlos.aleman@upc.edu.

Notes

The authors declare no competing financial interest.

ACKNOWLEDGMENTS

This work was supported by B. Braun Surgical S.A., by MICINN-FEDER funds (MAT2012-34498 and MAT2012-36205), and by the Generalitat de Catalunya (2009SGR925, 2009SGR1208 and XRQTC). Authors are indebted to CESCA for computational facilities.

REFERENCES

(1) Hench, L. L.; Wilson, J. Surface Active Materials. *Science* **1984**, *226*, 630−636.

(2) Hartgerink, J. D.; Beniash, E.; Stupp, S. I. Self-Assembly and Mineralization of Peptide-Amphiphile Nanofibers. *Science* **2001**, *294*, 1684−1688.

(3) Revilla-López, G.; Casanovas, J.; Bertran, O.; Turon, P.; Puiggalí, J.; Alemán, C. Modeling Biominerals Formed by Apatites and DNA. *Biointerphases* **2013**, *8*, 10−35.

(4) Bertran, O.; del Valle, L. J.; Revilla-López, G.; Chaves, G.; Cardus, Ll.; Casas, M. T.; Casanovas, J.; Turon, P.; Puiggalí, J.; Alemán. Mineralization of DNA into Nanoparticles of Hydroxyapatite. C. *Dalton Trans.* **2014**, *43*, 317−327.

(5) Martin-Pintado, N.; Yahyaee-Anzahaee, M.; Deleavey, G. F.; Portella, G.; Orozco, M.; Damha, M. J.; Gonzalez, C. Dramatic Effect of Furanose C2′-Substitution on Structure and Stability: Directing the Folding of the Human Telomeric Quadruplex with a Single Fluorine Atom. *J. Am. Chem. Soc.* **2013**, *135*, 5344−5347.

(6) Martin-Pintado, N.; Deleavey, G. F.; Portella, G.; Campos-Olivas, R.; Orozco, M.; Damha, M. J.; González, C. Backbone FC-H···O Hydrogen Bonds in 2′F-Substituted Nucleic Acids. *Angew. Chem., Int. Ed.* **2013**, *125*, 12065−12068.

(7) Altona, C.; Sundaralingam, M. Conformational Analysis of the Sugar Ring in Nucleosides and Nucleotides. New Description Using the Concept of Pseudorotation. *J. Am. Chem. Soc.* **1972**, *94*, 8205−8212.

(8) Altona, C.; Sundaralingam, M. Conformational Analysis of the Sugar Ring in Nucleosides and Nucleotides. Improved Method for the Interpretation of Proton Magnetic Resonance Coupling Constants. *J. Am. Chem. Soc.* **1973**, *95*, 2333−2344.

(9) Correll, C. C.; Wool, I. G.; Munishkin, A. The Two Faces of the Escherichia Coli 23SrRNA Sarcin/Ricin Domain: the Structure at 1.11 Å Resolution. *J. Mol. Biol.* **1999**, *292*, 275−287.

(10) Ban, N.; Nissen, P.; Hansen, J.; Moore, P. B.; Steitz, T. A. The Complete Atomic Structure of the Large Ribosomal Subunit at 2.4 Å Resolution. *Science* **2000**, *289*, 905−920.

(11) Ng, H. L.; Dickerson, R. E. Mediation of the A/B-DNA Helix Transition by G-Tracts in the Crystal Structure of Duplex CATGGGCCCATG. *Nucleic Acids Res.* **2002**, *30*, 4061−4067.

(12) Plavec, J.; Tong, W.; J. Chattopadhyaya, J. How Do the Gauche and Anomeric Effects Drive the Pseudorotational Equilibrium of the Pentofuranose Moiety of Nucleosides? *J. Am. Chem. Soc.* **1993**, *115*, 9734−9746.

(13) Brameld, K. A.; Goddard, W. A., III Ab Initio Quantum Mechanical Study of the Structures and Energies for the Pseudorotation of 5′-Dehydroxy Analogues of 2′-Deoxyribose and Ribose Sugars. *J. Am. Chem. Soc.* **1999**, *121*, 985−993.

(14) Pearlman, D. A.; Kollman, P. A. Evaluating the Assumptions Underlying Force Field Development and Application, Using Free Energy Conformational Maps for Nucleosides. *J. Am. Chem. Soc.* **1991**, *113*, 7167−7177.

(15) Barbe, S.; Bre, M. L. Effect of a Water Molecule on the Sugar Puckering of Uridine, 2′-Deoxyuridine, and 2′-O-Methyl Uridine Inserted in Duplexes. *J. Comput. Chem.* **2008**, *29*, 1353−1363.

(16) Rios-Font, R.; Bertrán, J.; Rodríguez-Santiago, L.; Sodupe, M. Effects of Ionization, Metal Cationization and Protonation on 2′-Deoxyguanosine: Changes on Sugar Puckering and Stability of the N-glycosidic Bond. *J. Phys. Chem. B* **2006**, *110*, 5767−5772.

(17) Vokacova, Z.; Matthias Bickelhaupt, F.; Sponer, J.; Sychrovsky, V. Structural Interpretation of J Coupling Constants in Guanosine and Deoxyguanosine: Modeling the Effects of Sugar Pucker, Backbone Conformation, and Base Pairing. *J. Phys. Chem. A* **2009**, *113*, 8379−8386.

(18) Boisbouvier, J.; Bryce, D. L.; O'Neil-Cabello, E.; Nikonowicz, E. P.; Bax, A. Resolution-Optimized NMR Measurement of 1DCH, 1DCC and 2DCH Residual Dipolar Couplings in Nucleic Acid Bases. *J. Biomol. NMR* **2004**, *30*, 287−301.

(19) Marino, J. P.; Landry, S. M.; Varani, G.; Tinoco, I. *J*-Coupling Restraints in RNA Structure Determination. *Acc. Chem. Res.* **1999**, *32*, 614−623.

(20) Munzarova, M. L.; Sklenar, V. DFT Analysis of NMR Scalar Interactions Across the Glycosidic Bond in DNA. *J. Am. Chem. Soc.* **2003**, *125*, 3649−3658.

(21) Sychrovsky, V.; Schneider, B.; Hobza, P.; Zidek, L.; Sklenar, V. The Effect of Water on NMR Spin−Spin Couplings in DNA: Improvement of Calculated Values by Application of Two Solvent Models. *Phys. Chem. Chem. Phys.* **2003**, *5*, 734−739.

(22) Bianchet, M. A.; Seiple, L. A.; Jiang, Y. L.; Ichikawa, Y.; Amzel, L. M.; Stivers, J. T. Electrostatic Guidance of Glycosyl Cation Migration Along the Reaction Coordinate of Uracil DNA Glycosylase. *Biochemistry* **2003**, *42*, 12455−12460.

(23) Hiughes, J. M.; Cameron, M.; Corwley, K. D. Structural Variations in Natural F, OH, and Cl Apatites. *Am. Mineral.* **1989**, *74*, 870−876.

(24) Phillips, J. C.; Braun, R.; Wang, W.; Gumbart, J.; Tajkhorshid, E.; Villa, E.; Chipot, C.; Skeel, R: D.; Kale, L.; Schulten, K. Scalable Molecular Dynamics with NAMD. *J. Comput. Chem.* **2005**, *26*, 1781−1802.

(25) Cornell, W. D.; Cieplak, P.; Bayly, C. I.; Gould, I. R.; Merz, K. M.; Ferguson, D. M.; Spellmeyer, D. C.; Fox, T.; Caldwell, J. W.; Kollman, P. A. A Second Generation Force Field for the Simulation of Proteins, Nucleic Acids, and Organic Molecules. *J. Am. Chem. Soc.* **1995**, *117*, 5179−5197.

(26) Duan, Y.; Chowdhury, S.; Lee, M. C.; Xiong, G.; Zhang, W.; Yang, R.; Cieplak, P.; Luo, R.; Lee, T.; Caldwell, J.; Wang, J.; Kollman, P. A. A Point-Charge Force Field for Molecular Mechanics Simulations of Proteins Based on Condensed-Phase Quantum Mechanical Calculations. *J. Comput. Chem.* **2003**, *24*, 1999−2012.

(27) Hornak, V.; Abel, R.; Okur, A.; Strockbine, B.; Roitberg, A.; Simmerling, C. Comparison of Multiple Amber Force Fields and Development of Improved Protein Backbone Parameters. *Proteins* **2006**, *65*, 712−725.

(28) Bradbrook, G. M.; Gleichmann, T.; Harrop, S. J.; Habash, J.; Raftery, J.; Kalb, J.; Yariv, J.; Hillier, I. H.; Helliwell, J. R. X-Ray and Molecular Dynamics Studies of Concanavalin-A Glucoside and Mannoside Complexes Relating Structure to Thermodynamics of Binding. *J. Chem. Soc. Faraday Trans.* **1998**, *94*, 1603−1611.

(29) Frisch, M. J.; Trucks, G. W.; Schlegel, H. B.; Scuseria, G. E.; Robb, M. A.; Cheeseman, J. R.; Scalmani, G.; Barone, V.; Mennucci, B.; Petersson, G. A.; Nakatsuji, H.; Caricato, M.; Li, X.; Hratchian, H. P.; Izmaylov, A. F.; Bloino, J.; Zheng, G.; Sonnenberg, J. L.; Hada, M.; Ehara, M.; Toyota, K.; Fukuda, R.; Hasegawa, J.; Ishida, M.; Nakajima, T.; Honda, Y.; Kitao, O.; Nakai, H.; Vreven, T.; Montgomery, J. A.; Jr.; Peralta, J. E.; Ogliaro, F.; Bearpark, M.; Heyd, J. J.; Brothers, E.; Kudin, K. N.; Staroverov, V. N.; Kobayashi, R.; Normand, J.; Raghavachari, K.; Rendell, A.; Burant, J. C.; Iyengar, S. S.; Tomasi, J.; Cossi, M.; Rega, N.; Millam, J. M.; Klene, M.; Knox, J. E.; Cross, J. B.; Bakken, V.; Adamo, C.; Jaramillo, J.; Gomperts, R.; Stratmann, R. E.; Yazyev, O.; Austin, A. J.; Cammi, R.; Pomelli, C.; Ochterski, J. W.; Martin, R. L.; Morokuma, K.; Zakrzewski, V. G.; Voth, G. A.; Salvador, P.; Dannenberg, J. J.; Dapprich, S.; Daniels, A. D.; Farkas, Ö.; Foresman, J. B.; Ortiz, J. V.; Cioslowski, J.; Fox, D. J. *Gaussian 09*, Revision A.1; Gaussian, Inc.: Wallingford CT, 2009.

(30) Clark, T.; Chandrasekhar, J.; Spitznagel, G. W.; von R. Schleyer, R. Efficient Diffuse Function-Augmented Basis Sets for Anion Calculations. III. The 3-21+G Basis Set for First-Row Elements, Li−F. *J. Comput. Chem.* **1983**, *4*, 294−301.

(31) Frisch, M. J.; Pople, J. A.; Binkley, J. S. Self-consistent Molecular-Orbital Methods. 25. Supplementary Functions for Gaussian-Basis Sets. *J. Chem. Phys.* **1984**, *80*, 3265−3269.

(32) Hariharan, P. C.; Pople, J. A. Influence of Polarization Functions on MO Hydrogenation Energies. *Theor. Chim. Acta* **1973**, *28*, 213−222.

(33) Becke, A. D. A New Mixing of Hartree–Fock and Local Density-Functional Theories. *J. Chem. Phys.* **1993**, *98*, 1372−1377.

(34) Lee, C.; Yang, W.; Parr, R. G. Development of the Colle-Salvetti Correlation-Energy Formula into a Functional of the Electron Density. *Phys. Rev. B* **1988**, *37*, 785−789.

(35) Grimme, S. Accurate Description of van der Waals Complexes by Density Functional Theory Including Empirical Corrections. *J. Comput. Chem.* **2004**, *25*, 1463−1473.

(36) Grimme, S. Semiempirical GGA-Type Density Functional Constructed with a Long-Range Dispersion Correction. *J. Comput. Chem.* **2006**, *27*, 1787−1799.
(37) Grimme, S.; Antony, J.; Ehrlich, S.; Krieg, H. A Consistent and Accurate Ab Initio Parametrization of Density Functional Dispersion Correction (DFT-D) for the 94 Elements H-Pu. *J. Chem. Phys.* **2010**, *132*, 154104.
(38) Mignon, P.; Ugliengo, P.; Sodupe, M. Theoretical Study of the Adsorption of RNA/DNA Based on the External Surfaces of Na^+-Montmorillonite. *J. Phys. Chem. C* **2009**, *113*, 13741−13749.
(39) Grzeskowiak, K.; Goodsell, D. S.; Kaczor-Grzeskowiak, M.; Cascio, D.; Dickerson, R. E. Crystallographic Analysis of C-C-A-A-G-C-T-T-G-G and Its Implications for Bending in B-DNA. *Biochemistry* **1993**, *32*, 8923−8931.
(40) de Leeuw, H. P. M.; Haasnot, C. A. G.; Altona, C. Empirical Correlations between Conformational Parameters in β-D-Furanoside Fragments Derived from a Statistical Survey of Crystal Structures of Nucleic Acid Constituents Full Description of Nucleoside Molecular Geometries in terms of Four Parameters. *Isr. J. Chem.* **1980**, *20*, 108−126.
(41) Hoffmann, R. A.; van Wijk, J.; Leeflang, B. R.; Makerling, J. P.; Altona, C.; Vliegenthart, J. F. G. Conformational Analysis of the α-L-Arabinofuranosides Present in Wheat Arabinoxylans from Proton-Proton Coupling Constants. *J. Am. Chem. Soc.* **1992**, *114*, 3710−3714.